Chinese Chemical Letters 34 (2023) 108507

Contents lists available at ScienceDirect

Chinese Chemical Letters

journal homepage: www.elsevier.com/locate/cclet

A NIR fluorescent probe for imaging thiophenol in the living system and revealing thiophenol-induced oxidative stress

Zesi Wang[a,1], Jiao Li[a,1], Jiao Chen[a,b], Zifeng Cao[a], Hui Li[a], Yaopeng Cao[a], Quanquan Li[a,c], Mengyao She[a,b], Ping Liu[a], Shengyong Zhang[a], Jianli Li[a,*]

[a] Key Laboratory of Synthetic and Natural Functional Molecule of the Ministry of Education, College of Chemistry & Materials Science, Northwest University, Xi'an 710127, China
[b] Key Laboratory of Resource Biology and Biotechnology in Western China, Ministry of Education, Biomedicine Key Laboratory of Shaanxi Province, Lab of Tissue Engineering, College of Life Sciences, Northwest University, Xi'an 710127, China
[c] Shaanxi Key Laboratory of Earth Surface System and Environmental Carrying Capacity, College of Urban and Environmental Sciences, Northwest University, Xi'an 710127, China

ARTICLE INFO

Article history:
Received 7 March 2023
Revised 20 April 2023
Accepted 23 April 2023
Available online 28 April 2023

Keywords:
Fluorescent probe
Near-infrared
Oxidative stress
Thiophenol
Large Stokes shift
Dicyanoisophorone

ABSTRACT

Thiophenol (PhSH) is an important raw material for organic synthesis, while its high toxicity to organisms makes it an environmental pollutant. Therefore, it is crucial to accurately detect PhSH and explore its metabolic process in the living system. Herein, a near-infrared (NIR) fluorescent probe **TEM-FB** was developed for sensing PhSH with a turn-on fluorescent signal at 719 nm and a large Stokes shift (198 nm) based on generating the intramolecular charge transfer (ICT) process. **TEM-FB** shows high specificity and significant sensitivity towards PhSH (detection limit: 10 nmol/L) *via* the aromatic nucleophilic substitution mechanism. Furthermore, it was successfully applied to image PhSH in multiple cell lines and in zebrafish. Notably, we revealed the oxidative stress process caused by PhSH and demonstrated that the hydrogen peroxide (H_2O_2) in cells would alleviate the poisonousness from exogenous PhSH for the first time. This work provides a promising bioimaging tool for monitoring PhSH in living systems and visualizing the process of oxidative stress induced by PhSH.

Thiophenol (PhSH) is a valuable intermediate in organic synthesis, which is widely utilized in the preparation of pharmaceuticals, agricultural chemicals, and various industrial products [1–5]. However, owing to high volatility, irritation, and toxicity [6,7], PhSH is listed as a priority pollutant by the U.S. Environmental Protection Agency. In biological systems, PhSH can be automatically oxidized to aromatic disulfide, and further induced oxidative stress with the production of harmful superoxide radicals and hydrogen peroxide (H_2O_2) [8]. Prolonged exposure time (>15 min) of PhSH would cause serious health problems [9], including central nervous system damage, breathing difficulties, vomiting, and even death [10–12]. Generally, the median lethal concentration (LC_{50}) of PhSH to fish ranged from 0.01 mmol/L to 0.4 mmol/L [13], to mice ranged from 2.15 mg/kg to 46.2 mg/kg [14]. Therefore, it is of great significance to develop a high-efficient method to monitor PhSH real-time in environmental and biological samples.

At present, some analytical methods have been reported to determine PhSH, such as high-performance liquid chromatography (HPLC) [15] and ultraviolet–visible (UV–vis) spectroscopy [16]. However, these methods have the disadvantages of time-consuming, low sensitivity, and complex pretreatment. Fluorescent probe is a popular tool for detecting various analytes due to the merit of its imaging capability *in situ*, superior selectivity, low detection limit, and non-inventiveness [17–25]. Significantly, fluorescent probes can be applied to investigate biological processes by tracking species in real-time within organisms [26–35]. Although many kinds of fluorescent probes have been developed to detect PhSH, some disadvantages still exist, such as low sensitivity, short fluorescence emission wavelength and short Stokes shift [36–54], which hindered their imaging application in the biological system (Table S1 in Supporting information). Given that the near-infrared (NIR) fluorescence features a higher signal-to-noise ratio and deeper tissue penetration [55–65], while the large Stokes shift can effectively reduce the interference caused by spontaneous fluorescence [66–69]. Therefore, it is valuable and desirable to develop PhSH specific fluorescent probe with both NIR emission and large Stokes shift.

* Corresponding author.
E-mail address: lijianli@nwu.edu.cn (J. Li).
[1] These authors contributed equally to this work.

https://doi.org/10.1016/j.cclet.2023.108507
1001-8417/

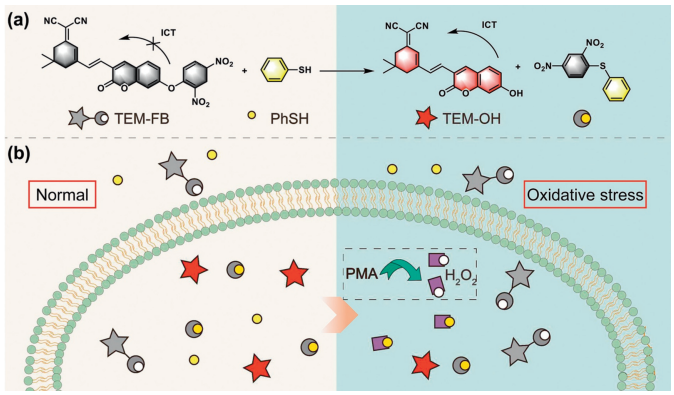

Fig. 1. (a) The designed fluorescent probe **TEM-FB** for detecting PhSH. (b) Schematic illustration of intracellular oxidative stress process induced by PhSH and the endogenous H_2O_2 alleviating the poison of PhSH. PMA, an inducer of endogenous ROS.

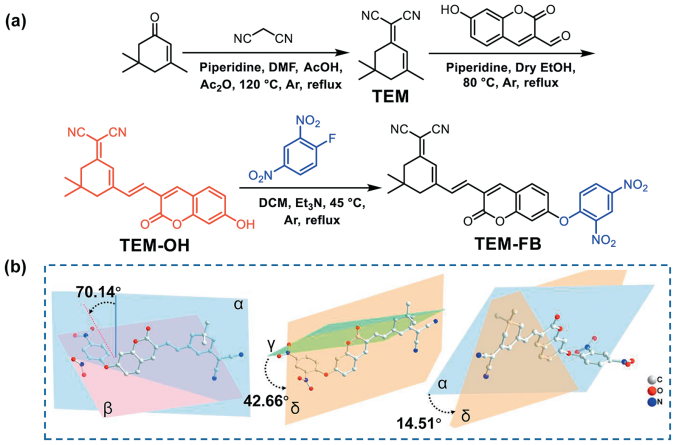

Fig. 2. (a) Synthesis route and (b) the crystal structure of **TEM-FB**.

Based on the above consideration and our previous work [70,71], herein, we bridged dicyanoisophorone and coumarin derivative to form a NIR fluorophore **TEM-OH** with a large Stokes shift (198 nm) and designed the fluorescent probe **TEM-FB** to detect PhSH *via* regulating intramolecular charge transfer (ICT) process (Fig. 1a). **TEM-FB** shows high specificity and sensitivity for sensing PhSH as well as exhibits prominent capability of visualizing exogenous PhSH in living cells and in zebrafish. Particularly, this work revealed the oxidative stress process induced by PhSH and proposed that H_2O_2 would alleviate the poisoning of PhSH (Fig. 1b).

To develop a NIR fluorescent probe for PhSH, the dicyanoisophorone and the coumarin derivative was conjugated to form a hydroxy–substituted NIR fluorophore **TEM-OH**. Then, the

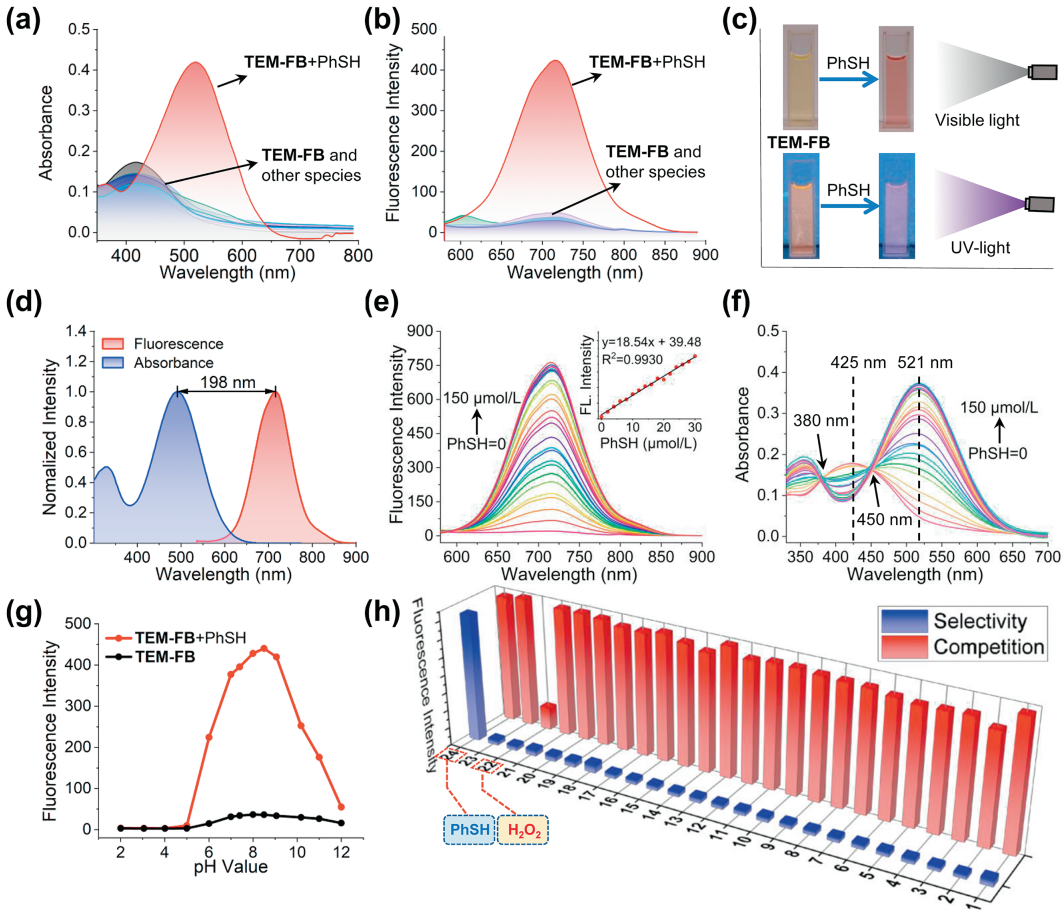

Fig. 3. (a) Ultraviolet absorbance and (b) fluorescence spectra of **TEM-FB** (10 μmol/L) upon the existence of various species (50 μmol/L) in DMSO/PBS (4:6, v/v, 10 mmol/L, pH 7.4). (c) Photographs of **TEM-FB** in the absence (left) and presence (right) of PhSH. (d) Normalized fluorescence and ultraviolet absorbance spectra of **TEM-FB** (10 μmol/L) upon the PhSH (50 μmol/L). (e) Fluorescence and (f) ultraviolet absorbance spectra of **TEM-FB** (10 μmol/L) upon the existence of PhSH (0–150 μmol/L). (g) The pH stability of **TEM-FB** (10 μmol/L) and **TEM-FB** (10 μmol/L) in presence of PhSH (50 μmol/L). (h) Fluorescence intensity of **TEM-FB** (10 μmol/L) in the presence of 1–24 (50 μmol/L) (1. Blank, 2. Lys, 3. Val, 4. Ile, 5. Phe, 6. Tau, 7. Thr, 8. Glu-Na, 9. Tyr, 10. NaCl, 11. $PbCl_2$, 12. $FeCl_2$, 13. Na_2SO_3, 14. KCl, 15. $NaHSO_3$, 16. $AlCl_3$, 17. NaHS, 18. Na_2S, 19. Cys, 20. GSH, 21. Hcy, 22. H_2O_2, 23. NaClO, 24. PhSH) (Blue columns); the fluorescence intensity of **TEM-FB** (10 μmol/L) in the presence of PhSH (50 μmol/L) and simultaneously existing 1–24 (50 μmol/L) (Red columns).

typical 2,4-dinitrophenyl was chosen as the fluorescence quenching unit and PhSH recognition unit to construct the target probe **TEM-FB** due to its strong withdraw-electron capability and potential reactivity to hydrosulfuryl species. **TEM-FB** was synthesized through a simple procedure (Fig. 2a and Figs. S1–S9 in Supporting information) and its crystal was obtained (Table S2 in Supporting information) (CCDC 2233985) in the solvent of PE/DCM = 1:2. As shown in Fig. 2b, the dihedral angle between the conjugate part plane (α) and the recognition unit plane (β) is 70.14° ($\theta_{\alpha\beta}$), which would promote to break ICT process. While the dihedral angle between plane γ and δ is measured to be $\theta_{\gamma\delta} = 42.66°$, and the segments of dicyanoisophorone and coumarin show a certain twist configuration ($\theta_{\alpha\delta} = 14.51°$), similarly, speculating fluorophore **TEM-OH** would not an absolute plane structure, thus effectively prevent fluorescence quenching caused by π-π stacking and improve its Stokes shift.

Experiments on fluorescence and UV–vis absorbance spectra of **TEM-FB** were performed in dimethyl sulfoxide/phosphate buffered saline (DMSO/PBS) (4:6, v/v, 10 mmol/L, pH 7.4), which solvent system was selected for the entire optical test because of its high fluorescence intensity (Fig. S10 in Supporting information). The reactivity of **TEM-FB** towards different analytes (including amino acids, metal ions, reactive sulfur species (RSS), reactive oxygen species (ROS), *etc.*) was tested. Encouragingly, **TEM-FB** exhibited a dramatic turn-on fluorescence emission at 719 nm with a 36-fold enhancement of fluorescence intensity only upon addition of PhSH. Simultaneously, the maximum peak of the UV–vis absorbance spectra red-shifted to 521 nm from 425 nm (Figs. 3a and b). Whereas negligible changes occurred in both in fluorescence and UV–vis absorbance upon addition of other species, the fact that even biothiols [cysteine (Cys), homocysteine (Hcy), glutathione (GSH) and NaHS] could not activate fluorescence signal manifests that **TEM-FB** endows excellent specificity for detecting PhSH. The vivid solution images also showed obvious changes in color and fluorescence before and after the response to PhSH (Fig. 3c). **TEM-FB** has a low fluorescence quantum yield $\Phi = 0.008$. Upon the interaction of it with PhSH, the quantum yield increases up to $\Phi = 0.076$. In addition, **TEM-FB** processes a large Stokes shift (~198 nm) (Fig. 3d) in response to PhSH, which can effectively avoid signal interference and fluorescence quenching caused by self-absorption.

To evaluate the quantitative detection capability of **TEM-FB** for PhSH, the fluorescence and absorbance titration experiment were performed by addition of different concentrations of PhSH (0–150 μmol/L) to **TEM-FB**. As shown in Fig. 3e, the fluorescence intensity at 719 nm were gradually increased upon addition of PhSH, and it displays an excellent linearity ($R^2 = 0.9930$) against the concentrations of PhSH ranging from 0 to 30 μmol/L. The limit of detection (LOD) was calculated to be 10 nmol/L according to the equation (LOD = 3 σ/k), which approximates to the half effective concentration (EC_{50}) reported in the literature [13]. Moreover, the absorbance at 521 nm also gradually elevated to a plateau until the concentration of PhSH up to 60 μmol/L (Fig. 3f). The results verified the promising quantitative ability of **TEM-FB** towards PhSH.

The kinetics experiment displayed that the fluorescent intensity (719 nm) of **TEM-FB** in the presence of PhSH increased rapidly from 0 to 30 min and then tended to be stable for approximately 60 min. Moreover, there almost no obvious changes of **TEM-FB** at 719 nm within 90 min, which indicates it possesses good stability (Fig. S11 in Supporting information).

To examine the practicability of **TEM-FB** in complex biological systems, the pH stability and anti-interference property were tested. As shown in Fig. 3g, there were slight changes in fluorescence intensity of **TEM-FB**, indicating high stability of **TEM-FB** in a wide pH scope (2.0–12.0). The **TEM-FB**+PhSH showed a significant fluorescence enhancement during pH = 7.0–9.0, which demonstrated that **TEM-FB** is effective at the physiological condition. The anti-interference ability of **TEM-FB**+PhSH upon addition of various other analytes were checked (Fig. 3h). Unexpectedly, the fluorescent intensity fluctuated indistinctively coexisting with all analytes but H_2O_2, which decreased remarkably. In this regard, we hypothesized that H_2O_2 may be a scavenger of PhSH.

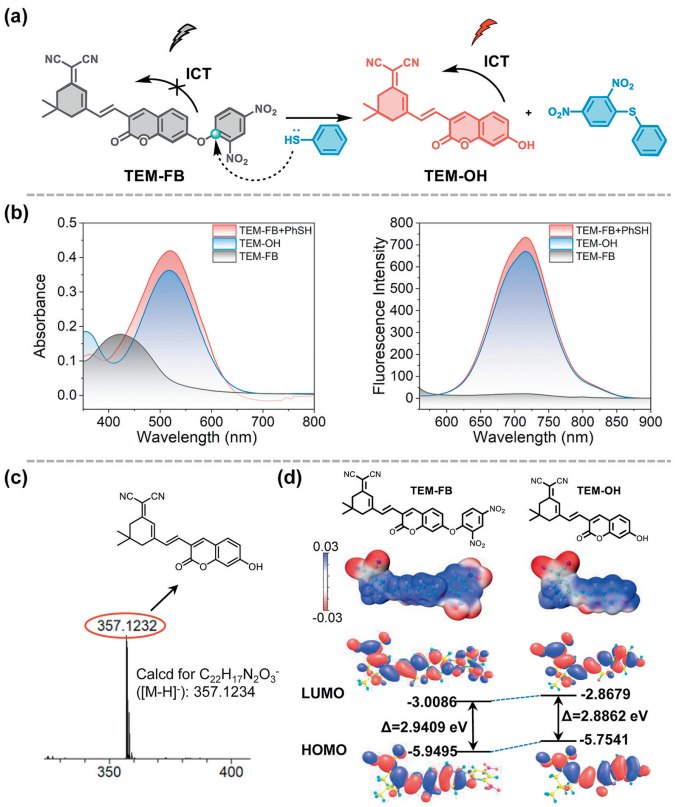

Fig. 4. (a) Proposed reaction mechanism of **TEM-FB** towards PhSH. (b) Ultraviolet absorbance and fluorescence spectra of **TEM-FB** (10 μmol/L) upon the existence of PhSH (50 μmol/L). (c) HRMS analysis of the mixture solution of **TEM-FB**+PhSH. (d) The electrostatic potential and the HOMO/LUMO gaps of **TEM-OH** and **TEM-FB**.

Afterwards, the recognition mechanism was explored. As shown in Fig. 4b, the fluorescence and UV–vis absorbance spectrum of the mixture solution of **TEM-FB** + PhSH were overlapped with the **TEM-OH**, indicating that **TEM-OH** is the production of **TEM-FB** and PhSH. This result is consistent with the peak at 357.1232 that analyzed by mass spectroscopy (Fig. 4c). Thus, we deduced the sensing mechanism is that PhSH attacks the carbon atom of **TEM-FB** through nucleophilic aromatic substitution reaction (S_NAr) and removes the recognition unit 2,4-dinitrophenyl group, which process would recover ICT characteristic accompanied with a dramatical fluorescence enhancement (Fig. 4a). Subsequently, the responses of **TEM-FB** to PhSH derivatives were evaluated. The results demonstrated that **TEM-FB** exhibited a significant response to thiophenol derivatives with electron-donating substituents, while demonstrating a weak or negligible response to those with electron-withdrawing substituents (Fig. S12 in Supporting information). This phenomenon would be attributed to the enhanced nucleophilicity of the sulfhydryl group of thiophenol derivatives with electron-donating substituents, as well as the diminished nucleophilicity of the sulfhydryl group of thiophenol derivatives with electron-withdrawing substituents.

Additionally, the electrostatic potential (ESP), the highest occupied molecular orbital (HOMO), and lowest unoccupied molecular orbital (LUMO) distribution of **TEM-OH** and **TEM-FB** were calculated to examine their ICT properties by density functional

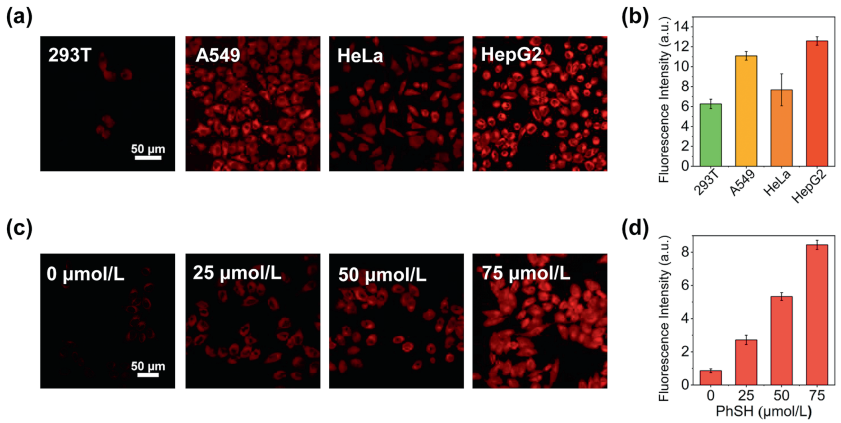

Fig. 5. (a) Fluorescence imaging of different living cell lines: 239T cells, A549 cells, HeLa cells, and HepG2 cells treated with PhSH (50 μmol/L) for 30 min before staining with **TEM-FB** (30 μmol/L) for 30 min. (b) Average fluorescence intensity. Data are presented as the mean ± SD ($n = 3$). (c) Fluorescence imaging of HepG2 cells treated with different concentrations of PhSH. (0, 25, 50, 75 μmol/L) for 30 min before staining with **TEM-FB** (30 μmol/L) for 30 min. (d) Average fluorescence intensity. Data are presented as the mean ± standard deviation (SD) ($n = 3$).

theory (DFT) [72,73]. As shown in Fig. 4d, the ESP of **TEM-FB** is negative to negative, destroying the push-pull electron system. While this pattern of **TEM-OH** is negative to positive, exhibiting excellent charge separation (negative in red and positive in blue) and thus it is in accord with ICT process. Furthermore, the HOMO of **TEM-FB** is merely distributed in the fluorophore unit, while its LUMO distribution are dispersed in fluorophore unit and recognition unit. Differently, both the HOMO and LUMO of **TEM-OH** are distributed in the conjugate unit, and the gaps of **TEM-OH** is lower than that of **TEM-FB**, manifesting that **TEM-FB** could serve as an ICT-based fluorescent probe.

Inspired by the above results *in vitro*, we further evaluated the capability of **TEM-FB** to image intracellular PhSH. First, MTT assay confirmed that **TEM-FB** almost caused no noticeable toxicity (Fig. S13 in Supporting information). Subsequently, fluorescence imaging in living cells (including normal cells (293T) and cancer cells (A549, HeLa, and HepG2)) were performed (Figs. 5a and b, Fig. S14 in Supporting information). Upon addition of **TEM-FB**, their displayed significant red fluorescence signals in living A549, HeLa, and HepG2 cells pretreated with PhSH (50 μmol/L). However, the fluorescence intensity in 293T cells were slight and lower than that in other cancer cells, which may be attributed to the low intake capacity of **TEM-FB** and PhSH by normal cells. Subsequently, HepG2 cells were stained with **TEM-FB** (30 μmol/L) followed by incubation with PhSH (0, 25, 50, and 75 μmol/L) for 30 min. As shown in Figs. 5c and d, an increased fluorescence intensity was observed with the increased PhSH concentration, which illustrates that **TEM-FB** could image different concentration of PhSH in living cancer cells.

Considering that the fluorescent intensity of **TEM-FB** for PhSH was greatly decreased in the presence of H_2O_2 *in vitro* experiments, and to validate our hypothesis mentioned above, we utilized **TEM-FB** to visualize the distribution of PhSH in the presence of exogenous H_2O_2 and endogenous H_2O_2 in living cells, respectively. In contrast with Fig. 6b, there are slight fluorescence signal observed when HepG2 cells treated with exogenous H_2O_2 or phorbol myristate acetate (PMA, an agent to induce endogenous ROS, including H_2O_2) in Figs. 6c and d, which similar to cells incubated with **TEM-FB** only (Figs. 6a and f). It suggested that H_2O_2 may eliminate PhSH in the living cells and alleviate PhSH poisoning. To investigate whether the toxic PhSH could trigger stress response by oxidative stress process, we examined the fluorescent signals of **TEM-FB** for PhSH in the living cells and the fixed cells, respectively. The fluorescence intensity in living cells (Fig. 6b) was observed lower than that in fixed cells (Figs. 6e and f), indicating that living cells occurred oxidative stress in the presence of PhSH accompanied with generating endogenous H_2O_2, while the fixed cells were difficult to occur this process. Consequently, it

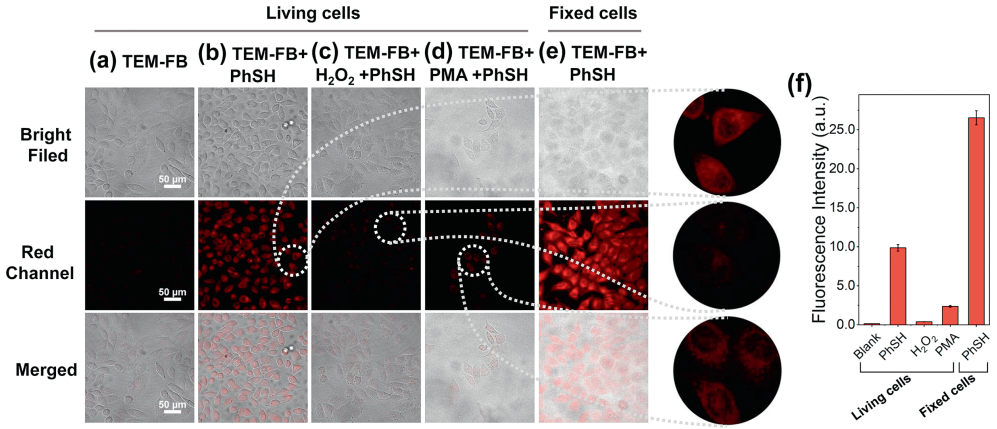

Fig. 6. Fluorescence imaging of HepG2 cells in different conditions (a) HepG2 cells were incubated with **TEM-FB** (30 μmol/L) for 30 min. (b) HepG2 cells were pretreated with PhSH (50 μmol/L) for 30 min before staining with **TEM-FB** (30 μmol/L) for 30 min. (c) HepG2 cells were pretreated with H_2O_2 (50 μmol/L) for 30 min and treated with PhSH (50 μmol/L) for 30 min before staining with **TEM-FB** (30 μmol/L) for 30 min. (d) HepG2 cells were pretreated with PMA (10 μg/mL) for 30 min and then treated with PhSH (50 μmol/L) for 30 min before staining with **TEM-FB** (30 μmol/L) for 30 min. (e) Fixed cells were pretreated with PhSH (50 μmol/L) for 30 min before incubating with **TEM-FB** (30 μmol/L) for 30 min. (f) Average fluorescence intensity. Data are presented as the mean ± SD ($n = 3$).

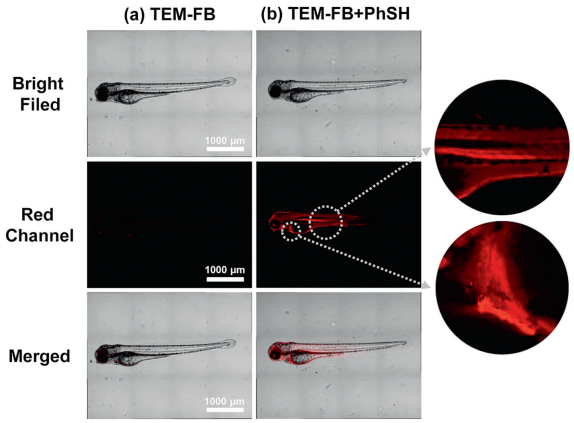

Fig. 7. Confocal fluorescence images of zebrafish in different conditions. (a) Zebrafish were pretreated with **TEM-FB** (30 μmol/L) for 30 min. (b) Zebrafish were pretreated with PhSH (50 μmol/L) for 30 min before incubating with **TEM-FB** (30 μmol/L) for 30 min.

revealed that H_2O_2 could alleviate PhSH poisoning by an oxidative stress process.

Given the promising imaging performance in live cells, the **TEM-FB** was further applied to image PhSH in zebrafish. All of animal experiments have been approved by the Animal Ethics Committee of Northwest University. It shows significant increase of fluorescence when zebrafish was incubated with **TEM-FB** and PhSH (Fig. 7b), while that incubated with **TEM-FB** only almost no fluorescence (Fig. 7a). Moreover, the liver and the intestine of zebrafish present higher fluorescence intensity than other regions, which may be related to **TEM-FB**/PhSH metabolism. The results demonstrated that **TEM-FB** could be used to perform PhSH imaging in living specimens with a high signal-to-noise ratio, and **TEM-FB**/PhSH is metabolized by the liver and digestive system of zebrafish.

In summary, we constructed an ICT-based NIR fluorescent probe **TEM-FB** for monitoring PhSH with large Stokes shift (198 nm) and high sensitivity (LOD = 10 nmol/L). **TEM-FB** displayed excellent capability of visualizing PhSH in living cells and in zebrafish with negligible cytotoxicity. Significantly, by using **TEM-FB**, we revealed that the oxidative stress process caused by PhSH and demonstrated that H_2O_2 in cells would alleviate the poisoning of PhSH for the first time. This work would provide a valuable tool for monitoring PhSH in physiological processes.

Declaration of competing interest

The authors declare that they have no known competing financial interests or personal relationships that could have appeared to influence the work reported in this paper.

Acknowledgments

This work was supported by the National Natural Science Foundation of China (Nos. 22077099 and 22171223), the Technology Innovation Leading Program of Shaanxi (No. 2020TG-031), the Innovation Capability Support Program of Shaanxi (Nos. 2023-CX-TD-75 and 2022KJXX-32), the Natural Science Basic Research Program of Shaanxi (No. 2023-JC-YB-141), and Young Talent Fund of Association for Science and Technology in Shaanxi, China (No. SWYY202206), and the Natural Science Basic Research Plan in Shaanxi Province of China (Nos. 2022JQ-151 and 2022JQ-125).

Supplementary materials

Supplementary material associated with this article can be found, in the online version, at doi:10.1016/j.cclet.2023.108507.

References

[1] C.W. Feng, D.Y. Wang, H.L. Lu, et al., Org. Lett. 24 (2022) 4485–4489.
[2] Q. Xiao, J.A. Burg, Y. Zhou, et al., Nano Lett. 18 (2018) 4900–4907.
[3] K. Shimada, K. Mitamura, J. Chromatogr. B: Biomed. Sci. Appl. 659 (1994) 227–241.
[4] Y. Hao, Q. Yin, Y. Zhang, et al., Molecules 24 (2019) 3716.
[5] M.A. Albakri, T.A. Saleh, Y. Mankour, et al., J. Colloid Interface Sci. 582 (2021) 428–438.
[6] M.M. Villalba, V.J. Litchfield, R.B. Smith, et al., J. Hazard. Mater. 154 (2008) 444–450.
[7] I.C. Popoff, J.R. Frank, C.B. Thanawalla, et al., J. Agric. Food Chem. 20 (1972) 80–82.
[8] R. Munday, J. Appl. Toxicol. 5 (1985) 402–408.
[9] Z. Wang, D.M. Han, W.P. Jia, et al., Anal. Chem. 84 (2012) 4915–4920.
[10] T.R. Juneja, R.L. Gupta, S. Samanta, Toxicol. Lett. 21 (1984) 185–189.
[11] R. Munday, J. Appl. Toxicol. 5 (1985) 409–413.
[12] P. Amrolia, S.G. Sullivan, A. Stern, et al., J. Appl. Toxicol. 9 (1989) 113–118.
[13] T.P. Heil, R.C. Lindsay, J. Environ. Sci. Health B 24 (1989) 349–360.
[14] F. Wu, H. Wang, J. Xu, et al., Sens. Actuators B: Chem. 254 (2018) 21–29.
[15] E.A. Mishalanie, J.W. Birks, Anal. Chem. 58 (1986) 918–923.
[16] Y. Shiraishi, K. Yamamoto, S. Sumiya, et al., Phys. Chem. Chem. Phys. 16 (2014) 12137–12142.
[17] W. Lu, S.F. Michelle, S. Aleksandar, et al., J. Am. Chem. Soc. 141 (2019) 2770–2781.
[18] W. Lu, T. Mai, D.E. Elisa, et al., Nat. Chem. 12 (2020) 165–172.
[19] B.G. Jonathan, K.M. Anand, L. Yajie, et al., Nat. Methods 14 (2017) 987–994.
[20] L. Gražvydas, R. Luc, U. Keitaro, et al., J. Am. Chem. Soc. 138 (2016) 9365–9368.
[21] L. Gražvydas, M. Gyuzel Yu, S. Sebastian, et al., Chem. Sci. 9 (2018) 3324–3334.
[22] N.B. Alexey, M. Gyuzel Yu, C.S. Sven, et al., Angew. Chem. Int. Ed. 55 (2016) 3290–3294.
[23] X. Chai, W. Zhu, Q. Meng, et al., Chin. Chem. Lett. 32 (2021) 210–213.
[24] G. Li, J. Wang, D. Li, et al., Chin. Chem. Lett. 32 (2021) 1527–1531.
[25] X. Ren, L. Liao, Z. Yang, et al., Chin. Chem. Lett. 32 (2021) 1061–1065.
[26] P. Zhou, M. She, P. Liu, et al., Sens. Actuators B: Chem. 318 (2020) 128258.
[27] W. Yao, Y. Cao, M. She, et al., ACS Sens. 6 (2021) 54–62.
[28] J. Chen, Z. Wang, M. She, et al., ACS Appl. Mater. Interfaces 11 (2019) 32605–32612.
[29] M. She, Z. Wang, J. Chen, et al., Coord. Chem. Rev. 432 (2021) 213712.
[30] J. Chen, D. Huang, M. She, et al., ACS Sens. 6 (2021) 628–640.
[31] H.W. Liu, L. Chen, C. Xu, et al., Chem. Soc. Rev. 47 (2018) 7140–7180.
[32] M.H. Lee, J.S. Kim, J.L. Sessler, Chem. Soc. Rev. 44 (2015) 4185–4191.
[33] P. Wang, H. Yang, C. Liu, et al., Chin. Chem. Lett. 32 (2021) 168–178.
[34] X. Li, H. Wang, Y. Zhang, et al., Chin. Chem. Lett. 32 (2021) 1541–1544.
[35] Z. Li, X. Xia, Y. You, et al., Chin. Chem. Lett. 32 (2021) 1785–1789.
[36] S. Erdemir, M. Oguz, S. Malkondu, Anal. Chim. Acta 1246 (2023) 340901.
[37] Y. Geng, H. Tian, L. Yang, et al., Sens. Actuators B: Chem. 273 (2018) 1670–1675.
[38] S.H. Guo, T.H. Leng, K. Wang, et al., Talanta 185 (2018) 359–364.
[39] G. Hu, Z. Wang, W. Yang, et al., Spectrochim. Acta A 272 (2022) 120984.
[40] Q. Liu, A. Li, X. Li, et al., Sens. Actuators B: Chem. 283 (2019) 820–830.
[41] H. Shang, H. Chen, Y. Tang, et al., Biosens. Bioelectron. 95 (2017) 81–86.
[42] J. Wu, D. Su, C. Qin, et al., Talanta 201 (2019) 111–118.
[43] Q. Wu, J. Wang, W. Liang, Dyes Pigm. 190 (2021) 109289.
[44] L. Xiao, D. Zhang, J. Zhang, et al., Tetrahedron 77 (2021) 131738.
[45] Q.Q. Yang, N. Ji, Y. Zhan, et al., Anal. Chim. Acta 1186 (2021) 339116.
[46] S. Zhang, Q. Wang, F. Wu, et al., Talanta 216 (2020) 120965.
[47] Y. Wu, A. Shi, H. Liu, et al., New J. Chem. 44 (2020) 17360–17367.
[48] X. Shao, R. Kang, Y. Zhang, et al., Anal. Chem. 87 (2015) 399–405.
[49] Y. Pan, T.B. Ren, D. Cheng, et al., Chem. Asian J. 11 (2016) 3575–3582.
[50] Z. Li, Y. Wu, Y. Shen, et al., ACS Omega 5 (2020) 10808–10814.
[51] D. Yu, F. Huang, S. Ding, et al., Anal. Chem. 86 (2014) 8835–8841.
[52] C. Zhao, Y. Zhou, Q. Lin, et al., J. Phys. Chem. B 115 (2011) 642–647.
[53] J. Niu, Y. Li, R. Zhang, et al., Chem. Commun. 57 (2021) 2800–2803.
[54] X. Liu, F. Qi, Y. Su, et al., J. Mater. Chem. C 4 (2016) 4320–4326.
[55] G. Lukinavičius, K. Umezawa, N. Olivier, et al., Nat. Chem. 5 (2013) 132–139.
[56] E.D. Cosco, A.L. Spearman, S. Ramakrishnan, et al., Nat. Chem. 12 (2020) 1123–1130.
[57] N.M. Htun, Y.C. Chen, B. Lim, et al., Nat. Commun. 8 (2017) 75.
[58] K.S. de Valk, H.J. Handgraaf, M.M. Deken, et al., Nat. Commun. 10 (2019) 3118.
[59] L.A. Kasatkina, C. Ma, M.E. Matlashov, et al., Nat. Commun. 13 (2022) 2813.
[60] D.M. Shcherbakova, M. Baloban, A.V. Emelyanov, et al., Nat. Commun. 7 (2016) 12405.
[61] X. Luo, J. Li, J. Zhao, et al., Chin. Chem. Lett. 30 (2019) 839–846.
[62] L. Feng, Z. Tian, M. Zhang, et al., Chin. Chem. Lett. 32 (2021) 3053–3056.
[63] W. Huili, S. Yishuo, L. Xuemei, et al., Chin. Chem. Lett. 34 (2023) 107626.
[64] X. Ma, Y. Huang, A. Abedi Syed Ali, et al., CCS Chem. 4 (2022) 1961–1976.
[65] X. Ma, Y. Huang, W. Chen, et al., Angew. Chem. Int. Ed. 62 (2023) e202216109.
[66] G. Jiang, T.B. Ren, E. D'Este, et al., Nat. Commun. 13 (2022) 2264.
[67] M. Mieczkowski, C. Steinmetzger, I. Bessi, et al., Nat. Commun. 12 (2021) 3549.
[68] R. Wang, J. Chen, J. Gao, et al., Chem. Sci. 10 (2019) 7222–7227.
[69] S. Zhou, Y. Rong, H. Wang, et al., Sens. Actuators B: Chem. 276 (2018) 136–141.
[70] J. Chen, Y. Li, X. Feng, et al., Spectrochim. Acta A 246 (2021) 119041–119047.
[71] M. She, Z. Wang, T. Luo, et al., Chem. Sci. 9 (2018) 8065–8070.
[72] T. Lu, F. Chen, J. Comput. Chem. 33 (2012) 580–592.
[73] J. Zhang, T. Lu, PCCP 23 (2021) 20323–20328.